Electronic structure and magnetic anisotropy transition in $Mn_{3-x}Co_xGa$ Heusler films investigated with soft x-ray spectroscopy

Seungho Seong [1], Yeonji Seo [1], Geum Ha Lim,[1] Woosuk Yoo,[2] Myung-Hwa Jung [2], Younghak Kim [3],
Sang Wook Han [4], and J.-S. Kang [1,*]

[1]*Department of Physics, The Catholic University of Korea (CUK), Bucheon 14662, Korea*
[2]*Department of Physics, Sogang University, Seoul 04107, Korea*
[3]*Pohang Accelerator Laboratory (PAL), POSTECH, Pohang 37673, Korea*
[4]*Basic Science Research Institute, University of Ulsan, Ulsan 44610, Korea*

Employing soft x-ray magnetic circular dichroism (XMCD) and soft x-ray absorption spectroscopy (XAS), we have investigated electronic structures and spin configurations of Co-substituted Mn_3Ga ($Mn_{3-x}Co_xGa$) Heusler films, which are promising spintronic materials exhibiting perpendicular magnetic anisotropy (PMA). Co $2p$ XAS and XMCD measurements, combined with the charge-transfer multiplet analysis, show that the substituted Co ions in $Mn_{3-x}Co_xGa$ consist of mainly ferromagnetic metallic Co clusters and a small amount of divalent Co ions with disordered magnetic moments. Mn $2p$ XAS and XMCD measurements show that Mn ions at both the octahedral and tetrahedral sites in $Mn_{3-x}Co_xGa$ are nearly divalent with weak covalent-bonding nature, reflecting non-Jahn-Teller ions, and that the magnetic moments of Mn ions are polarized along the ordered magnetic moments of the substituted Co ions. Angle-dependent Co $2p$ XMCD data of $Mn_{3-x}Co_xGa$ agree with the weak magnetic anisotropy transition from PMA to in-plane magnetic anisotropy (IMA) with increasing x. Spin and orbital magnetic moments of Co ions are estimated by using the sum-rule analysis, which reveal negligible Co-content and polar-angle dependencies of the Co orbital to spin magnetic moment ratio. This work reveals that the PMA-to-IMA magnetic transition in $Mn_{3-x}Co_xGa$ is determined mainly by ferromagnetic metallic Co clusters.

I. INTRODUCTION

Heusler compounds have attracted much attention due to the predicted half-metallic electronic structures [1], as well as diverse physical properties, such as ferromagnetic, ferrimagnetic, semiconducting, insulating, superconducting, and topological insulator properties [2–5]. Half-metallic ferromagnets are known to have 100% spin polarization at the Fermi level (E_F) [1]. A magnetically ordered half metal with vanishing magnetization is called as a compensated half-metallic ferrimagnet, which is very important in spintronic device application [6–9]. According to the Slater-Pauling plot for a series of $L2_1$ Heusler compounds, the moment disappears when there are 24 valence electrons per formula [4]. Indeed artificially-synthesized cubic Mn_3Ga Heusler, which has 24 valence electrons, was considered to be a potential compensated half-metallic ferrimagnet [4,6], in which the vanishing magnetization arises from the compensation of the different sublattice moments [see Fig. 1(c)].

Among possible candidates for spintronic applications, extensive studies were reported for Mn_3Ga Heusler films due to their high spin polarization ($P \sim 58\%$), high perpendicular magnetic anisotropy (PMA), and low saturation magnetization (M_S) [4,10–13]. For practical applications, however, it is required to reduce the coercivity H_C in Mn_3Ga while

maintaining high PMA. To achieve such properties, substituting $3d$ transition-metal (TM) elements in Mn_3Ga was attempted [14–16]. Among TM substitutions, Co-substituted $Mn_{3-x}Co_xGa$ films exhibited a magnetic transition from hard ferrimagnetism with PMA to soft ferrimagnetism with in-plane magnetic anisotropy (IMA) as the Co content (x) increases [16]. In addition, significantly low H_C, relatively low M_S, and the PMA were observed in the critical regime of $Mn_{3-x}Co_xGa$ ($\sim 0.3 \leqslant x \leqslant \sim 0.6$) [16] [see Fig. 1(d)]. In order to understand the origin of the PMA-to-IMA transition and the interesting magnetic properties in the critical regime, it is necessary to investigate the local electronic structure of $Mn_{3-x}Co_xGa$.

Soft x-ray absorption spectroscopy (XAS) [17,18] and soft x-ray magnetic circular dichroism (XMCD)[19,20] are very powerful experimental tools for studying the site-specific local electronic structures of TM ions in TM-based compounds. TM L-edge ($2p$) XAS provides a direct information on their valence states because the TM $2p \rightarrow 3d$ absorption process is involved in TM $2p$ XAS. On the other hand, XMCD is a very unique spectroscopic experiment that can provide the microscopic information on the spin and orbital components of the element-specific local magnetic moments of ferromagnetic TM ions separately [19,20]. Note that TM $3d$ electrons are very important in determining the magnetic properties of the TM oxides. Indeed, TM $2p$ XAS and XMCD provided a crucial information on the half-metallic ferromagnet [21].
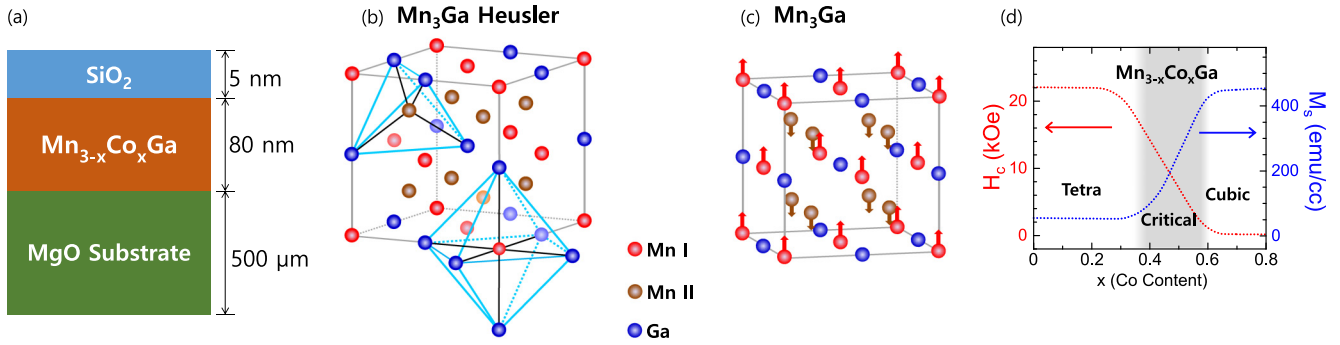
*kangjs@catholic.ac.kr

FIG. 1. Crystal structure and the Magnetic properties of $Mn_{3-x}Co_xGa$ Heusler films. (a) The schematic drawing (geometrical configuration) of $Mn_{3-x}Co_xGa$ film samples. (b) Inverse Heusler structure of Mn_3Ga, showing the local octahedral (O_h) symmetry of a Mn I site and the tetrahedral (T_d) symmetry of a Mn II site. (c) Magnetic structure of cubic Heusler Mn_3Ga, where the arrows represent the directions of the magnetic moments. In $Mn_{3-x}Co_xGa$, Co ions are considered to go into Mn II sites [16]. (d) Coercivity (H_C) and remanent magnetization (M_s) vs the Co concentration (x) in $Mn_{3-x}Co_xGa$ films (reproduced from Ref. [16]), where the label "Tetra" denotes the tetragonal structure.

A few XAS and XMCD studies were reported for $Mn_{3-x}Co_xGa$ films [22–24] as well as undoped Mn_3Ga films [25,26], and also for related Heulser compounds [27,28]. However, the origin of the PMA-to-IMA transition and the accompanying magnetic properties in $Mn_{3-x}Co_xGa$ has not been well understood yet. In this work, we have investigated the local electronic structures of $Mn_{3-x}Co_xGa$ Heusler films by employing angle-dependent XMCD and XAS.

II. EXPERIMENTAL DETAILS

$Mn_{3-x}Co_xGa$ film samples were deposited on MgO (001) substrates by using DC/RF magnetron sputtering, and SiO_2 capping layer was deposited on top of $Mn_{3-x}Co_xGa$ films [see Fig. 1(a)]. These films were deposited by cosputtering three targets of Mn_2Ga, Mn, and Co. The crystal structure and the Co content (x) were determined by x-ray diffraction (XRD) and energy-dispersive spectroscopy (EDC) in scanning electron microscopy (SEM), respectively. The details of the sample growth and characterization are described in Ref. [16].

XAS and XMCD experiments were performed at the 2A elliptically polarized undulator beamline of the Pohang Light Source (PLS). XAS and XMCD spectra were obtained by total electron yield (TEY) mode via sample drain current. To obtain XMCD spectra, the external magnetic field of $H \sim 0.7$ T (0.67 T) was applied. For XMCD measurements, the two absorption spectra of ρ_+ and ρ_- were obtained with the right and left circularly polarized photons, respectively. Then the XMCD spectrum ($\Delta\rho$) was obtained by taking a difference between the absorption intensities with different photon helicities at each photon energy, i.e., $\Delta\rho \equiv \rho^+ - \rho^-$. The total instrumental resolution for XAS and XMCD was set at ≈ 100 meV at $h\nu \sim 600$ eV. The base pressure was better than 3×10^{-10} Torr. All the XAS/XMCD data presented in this work were obtained at room temperature [29]. All the XAS/XMCD spectra were normalized to the incident photon flux.

III. RESULTS AND DISCUSSION

Figure 2 shows the measured Co $2p$ (L-edge) XAS and XMCD spectra of $Mn_{3-x}Co_xGa$. In Fig. 2(a), are shown the Co $2p$ XAS spectra of $Mn_{3-x}Co_xGa$ ($x = 0.17, 0.56, 0.77$), which are scaled at the Co $2p_{3/2}$ (L_3) peaks. Even though the line shape of $x = 0.17$ is very noisy due to the small Co concentration, the line shapes of $x = 0.56$ and 0.77 are similar to each other. This comparison indicates that the valence states of the substituted Co ions do not change for different Co concentrations (x) in $Mn_{3-x}Co_xGa$.

Figure 2(b) compares a typical Co $2p$ XAS spectrum of $Mn_{3-x}Co_xGa$ ($x = 0.56$) with those of reference Co materials, such as Co metal [20], divalent CoO (Co^{2+}, O_h) [30], divalent $CoCr_2O_4$ (Co^{2+}, T_d) (our data), $Ce_3Co_4Sn_{13}$ ($h\nu$ shifted by 0.5 eV) [31], and trivalent $AgCoO_2$ (Co^{3+}) [32]. The Co $2p$ XAS spectrum of $Mn_{3-x}Co_xGa$ is rather similar to that of Co metal, except for the bumps at higher $h\nu$ sides of the main peaks ($h\nu \sim 783$ and ~ 800 eV), and that of $Ce_3Co_4Sn_{13}$, but it is quite different from that of trivalent $AgCoO_2$ (Co3+). According to the original work for $Ce_3Co_4Sn_{13}$ [31], the Co ions in $Ce_3Co_4Sn_{13}$ are interpreted to be trivalent under the trigonal prism geometry based on the cluster model calculations. However, the energies of the Co $2p$ XAS peaks of $Ce_3Co_4Sn_{13}$ are lower than those of trivalent Co materials but close to those of divalent Co oxides and Co metal, indicating that the valence states of the Co ions in $Ce_3Co_4Sn_{13}$ are not trivalent but are probably close to being divalent. Hence, the finding in Fig. 2(b) suggests that a large portion of the substituted Co ions form metallic clusters locally [see Fig. 2(g)].

In order to determine the valence states of the Co ions, in Figs. 2(c)–2(e) are compared the Co $2p$ XAS spectrum of a the representative $Mn_{3-x}Co_xGa$ ($x = 0.56$) with those of Co metal (top), $CoCr_2O_4$ (Co^{2+}, T_d) (middle), and the calculated Co $2p$ XAS for Co^{2+} (T_d), respectively, by superposing two spectra onto each other. Here Co metal and $CoCr_2O_4$ (Co^{2+}, T_d) are chosen to represent a metallic-bonding system and an ionic-bonding system, respectively. The calculations are performed based on the *ab initio* configuration-interaction (CI) cluster model and the charge transfer multiplet (CTM)
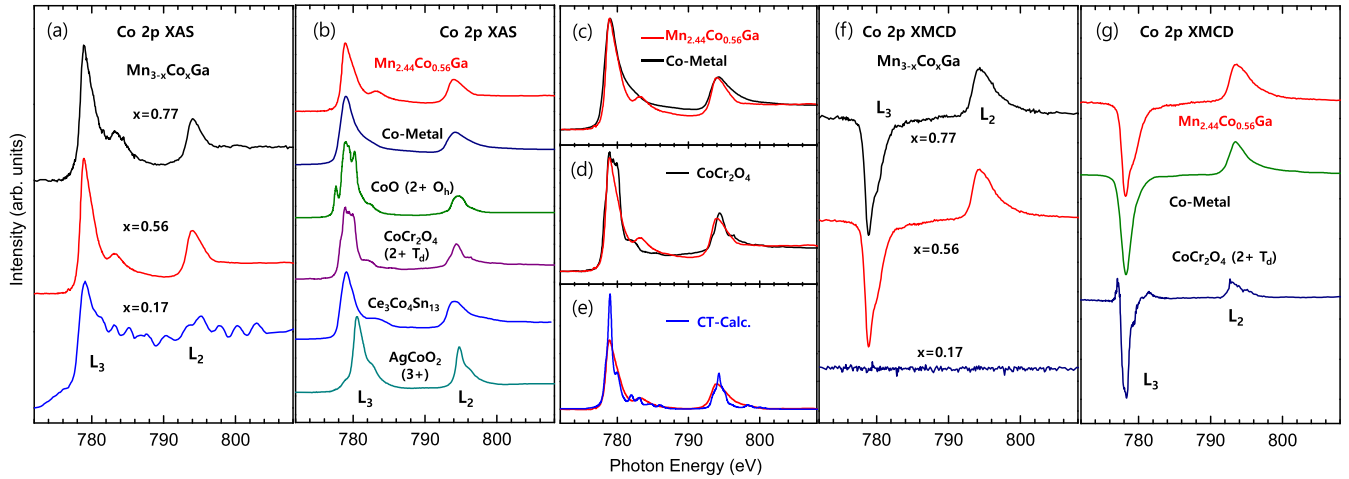
FIG. 2. Co $2p$ XAS and XMCD spectra of $Mn_{3-x}Co_xGa$. (a) Comparison of the Co $2p$ XAS spectra of $Mn_{3-x}Co_xGa$ ($x = 0.17$, 0.56, 0.77), scaled at the $2p_{3/2}$ (L_3) peaks. (b) Comparison of a typical Co $2p$ XAS spectrum of $Mn_{3-x}Co_xGa$ ($x = 0.56$) with those of reference Co materials, such as Co metal, CoO (Co^{2+}, O_h), $CoCr_2O_4$ (Co^{2+}, T_d), $Ce_3Co_4Sn_{13}$ ($h\nu' = h\nu - 0.5$ eV), and $AgCoO_2$ (Co^{3+}, O_h). (c),(d) Comparison of the Co $2p$ XAS line shapes of $Mn_{3-x}Co_xGa$ ($x = 0.56$) with those of Co metal and $CoCr_2O_4$ (Co^{2+}, T_d), respectively. (e) Comparison of the background-subtracted Co $2p$ XAS spectrum of $Mn_{3-x}Co_xGa$ ($x = 0.56$) with the calculated Co $2p$ XAS for Co^{2+} (T_d), obtained from the charge-transfer (CT) multiplet calculations. (f) Comparison of the Co $2p$ XMCD spectra of $Mn_{3-x}Co_xGa$ ($x = 0.17$, 0.56, 0.77), normalized to the Co $2p_{3/2}$ XAS peak intensities. (g) Comparison of a typical Co $2p$ XMCD spectrum of $Mn_{3-x}Co_xGa$ ($x = 0.56$) with those of ferromagnetic Co metal and ferrimagnetic spinel $CoCr_2O_4$ (Co^{2+}).

approach [33]. In Fig. 2(e), the background of the measured Co $2p$ XAS spectrum is removed because the background is not implemented in calculations. In the CI model for T_d symmetry, the free atomic multiplets due to the four near-neighbor anion environment are determined by the crystal field, which splits the energy levels of $3d$ orbitals, and the hybridization, which takes account of the covalency between Co $3d$ and anion sp states [33,34]. The parameters employed in this fitting are as follows: $10Dq = 1.5$ eV, $\Delta = 1.0$ eV, $U_{dd} = 5$ eV, $U_{pd} = 7$ eV, $T(b_1) = T(b_2) = T(e) = 1.4$ eV, $T(a_1) = 0.5$ eV, where $10Dq$: the crystal-field splitting energy, corresponding to the energy separation between t_{2g} and e_g orbitals, Δ: the charge transfer energy between $3d^n$ and $3d^{n+1}\bar{L}$ ($\bar{L}$: a ligand hole), U_{dd}: the repulsive $3d$-$3d$ Coulomb interaction, U_{pd}: the attractive $2p$-$3d$ Coulomb interaction, $T(b_1)$, $T(b_2)$, $T(e)$, $T(a_1)$: the hopping integrals between the ligand states and $3d$ orbitals (b_1, b_2, e, a_1). The details of the calculations and the meaning of the fitting parameters are described in Refs. [34–36].

Figures 2(c) and 2(d) show that the measured Co $2p$ XAS spectrum of $Mn_{3-x}Co_xGa$ is more similar to that of Co metal than that of divalent T_d $CoCr_2O_4$, while Fig. 2(e) suggests that it can still be described reasonably well by the divalent Co^{2+} ion under the T_d symmetry, where the charge transfer effect is included. Nevertheless, as shown in Fig. 2(g), the measured Co $2p$ XMCD spectrum of $Mn_{3-x}Co_xGa$ is more similar to that of Co metal than that of the covalent-bonded Co^{2+} states under the T_d symmetry. Hence, we interpret that the Co $2p$ XAS spectrum of $Mn_{3-x}Co_xGa$ is a mixture of the metallic states and the covalent-bonded states.

The observed high-energy shoulders in Co $2p$ XAS of $Mn_{3-x}Co_xGa$ ($h\nu \sim 783$ and ~ 800 eV) are similar to those in $Mn_{1.8}Co_{1.2}Ga$ [24], Co_2MnGa [27], and Mn_2CoSn [28]. However, Co $2p$ XMCD spectra of $Mn_{3-x}Co_xGa$ [see Fig. 2(g)] are very metallic-like. Hence, we assign the main

$2p_{3/2}$ (L_3) and $2p_{1/2}$ (L_2) peaks (~ 779 and ~ 794 eV) and the high-energy shoulders (~ 783 and ~ 800 eV) in the measured Co $2p$ XAS of $Mn_{3-x}Co_xGa$ to represent the metallic states and the covalent-bonded states (or the Co-Ga hybridized states), respectively. This interpretation is supported by the Co $2p$ XMCD spectra, shown in Figs. 2(f) and 2(g).

In Fig. 2(f), the Co $2p$ XMCD spectra of $Mn_{3-x}Co_xGa$ ($x = 0.17$, 0.56, 0.77) are shown, normalized to the Co $2p_{3/2}$ XAS peaks. The Co $2p$ XMCD spectra of $x = 0.56$ and 0.77 are very similar to each other, and exhibit nearly single peak for each of $2p_{3/2}$ and $2p_{1/2}$ components, i.e., very weak multiplet features. On the other hand, the Co $2p$ XMCD intensity of $x = 0.17$ is very weak, indicating almost negligible spin polarization of Co ions. In order to determine the spin configurations of Co ions in $Mn_{3-x}Co_xGa$, we have compared a representative Co $2p$ XMCD spectrum of $Mn_{3-x}Co_xGa$ ($x = 0.56$) with those of reference Co materials in Fig. 2(g), where ferromagnetic Co metal and ferrimagnetic spinel $CoCr_2O_4$ (Co^{2+}, T_d) are chosen as reference materials. The Co $2p$ XMCD spectrum of $Mn_{3-x}Co_xGa$ is different from that of $CoCr_2O_4$, which reveals sharp multiplet structures, but it is more similar to that of Co metal except for the weak extra feature of a higher-energy shoulders ($h\nu \sim 780$ eV).

The comparisons in Figs. 2(f) and 2(g) indicate that (i) both the valence and spin states of the Co ions in $Mn_{3-x}Co_xGa$ do not change as x varies, (ii) Co ions are ordered ferromagnetically, and (iii) most of them form metallic clusters, the bonding of which is far from being ionic. Note that there are no XMCD signals corresponding to the covalent-bonded Co ions [$h\nu \sim 783$ eV in Figs. 2(a)–2(c)], implying that the magnetic moments of the covalent-bonded Co ions are disordered. Hence the findings in Co $2p$ XMCD support our interpretation of Co $2p$ XAS [see Figs. 2(c)–2(e)]. Thus, based on the Co $2p$ XAS and XMCD data, we conclude that the substituted Co ions in $Mn_{3-x}Co_xGa$ are composed of a mixture of the

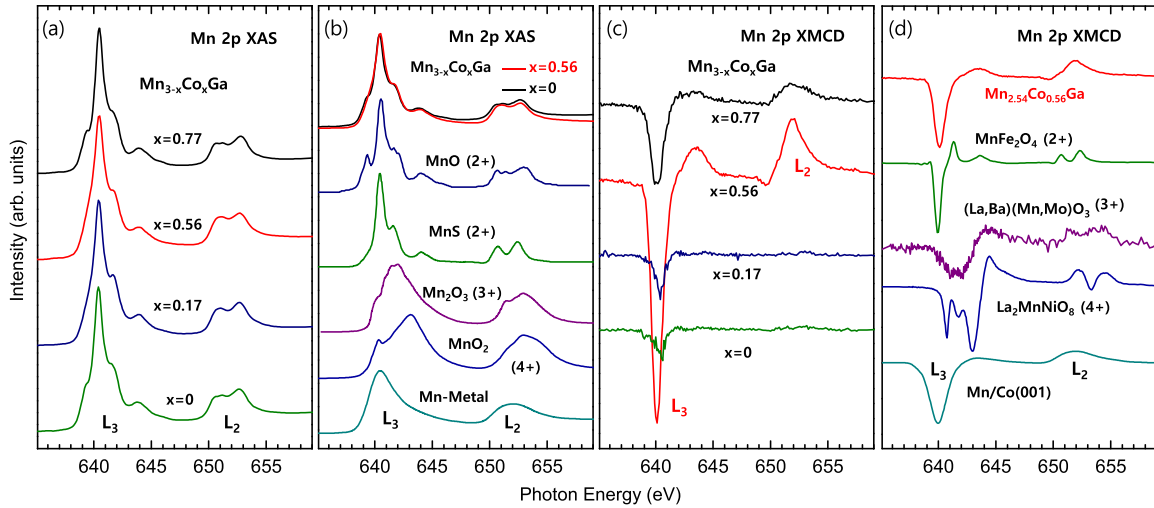FIG. 3. Mn $2p$ XAS and XMCD spectra of $Mn_{3-x}Co_xGa$. (a) Comparison of the Mn $2p$ XAS spectra of $Mn_{3-x}Co_xGa$ ($x = 0$, 0.17, 0.56, 0.77), scaled at the $2p_{3/2}$ peaks. (b) Comparison of a typical Mn $2p$ XAS spectrum of $Mn_{3-x}Co_xGa$ ($x = 0.56$) with those of MnO (Mn 2+, O_h), MnS (Mn 2+, T_d), Mn_2O_3 (Mn 3+), MnO_2 (Mn 4+), and that of Mn metal. (c) Comparison of the Mn $2p$ XMCD spectra of $Mn_{3-x}Co_xGa$ ($x = 0$, 0.17, 0.56, 0.77), normalized to the Mn $2p_{3/2}$ XAS peaks. (d) Comparison of a typical Mn $2p$ XMCD spectrum of $Mn_{3-x}Co_xGa$ ($x = 0.56$) with those of reference Mn oxides, such as divalent (Mn^{2+}) $MnFe_2O_4$, trivalent (Mn^{3+}) $La_{1-3x}Ba_{3x}Mn_{1-x}Mo_xO_3$ ($x = 0.03$) ($\equiv$ (La, Ba)(Mn, Mo)O_3), tetravalent (Mn^{4+}) La_2MnNiO_6, and metallic Mn(1 monolayer)/Co(001) film ($\equiv$ Mn/Co(001)).

ferromangetic metallic clusters and the covalent-bonded ions with disordered magnetic moments. Negligible Co $2p$ XMCD for $x = 0.17$ also indicates that the substituted Co ions initially go into T_d sites for small x, but tend to form the Co clusters for larger x.

Figure 3 shows the measured Mn $2p$ XAS and XMCD spectra of $Mn_{3-x}Co_xGa$. In Fig. 3(a) the Mn $2p$ XAS spectra of $Mn_{3-x}Co_xGa$ ($x = 0$, 0.17, 0.56, 0.77) are compared, scaled at the Mn $2p_{3/2}$ peaks. This comparison shows that the line shapes of the Mn $2p$ XAS spectra are very similar to one another for different x values, indicating that the valence states of Mn ions do not change with the Co concentration (x).

In order to determine the valence states of Mn ions in $Mn_{3-x}Co_xGa$, we have compared the Mn $2p$ XAS spectra of $Mn_{3-x}Co_xGa$ ($x = 0$, 0.56) with those of reference Mn materials in Fig. 3(b). Here are included MnO (Mn^{2+}, O_h) [37], MnS (Mn^{2+}, T_d) [38], Mn_2O_3 (Mn^{3+}) [39], MnO_2 (Mn^{4+}) [39], and Mn metal (our data). The Mn $2p$ XAS spectra of $Mn_{3-x}Co_xGa$ are found to be very similar to that of divalent MnO, but quite different from those of trivalent Mn_2O_3 and tetravalent MnO_2, indicating that the valence states of the Mn ions in $Mn_{3-x}Co_xGa$ are nearly divalent.

The multiplet features in Mn $2p$ XAS spectra of $Mn_{3-x}Co_xGa$ in this work are similar to those of MnO and MnS, while those of other Heusler compounds, such as $Mn_{2.2}Co_{0.8}Ga$ [22], $Mn_{1.8}Co_{1.2}Ga$ [24], Co_2MnGa [27], and Mn_2CoSn [28] are less structured. Considering the probing depth of XAS collected in the TEY mode ($\sim$50 Å) [40] in this work, the similarity of XAS of $Mn_{3-x}Co_xGa$ to that of MnO seems to indicate a partial oxidation of Mn ions in $Mn_{3-x}Co_xGa$ films. The weaker pre-peak feature in L_3 ($\sim$639 eV) and the weaker central peak in L_2 in $Mn_{3-x}Co_xGa$, as compared to MnO, suggest that part of the Mn atoms that are near the SiO_2-$Mn_{3-x}Co_xGa$ interface are oxidized. This also explains why the L_3 pre-peak ($\sim$639 eV) and the

central L_2 peak do not develop systematically with increasing x, reflecting a certain scattering of the oxidized Mn atoms.

According to our previous line shape-analysis of the Mn $2p$ XAS spectrum of $Mn_{3-x}Co_xGa$ [23], the Mn $2p$ XAS spectra of $Mn_{3-x}Co_xGa$ reflect the mixture of two different Mn sites, i.e., the O_h site with six Ga neighbors, and the T_d site with four Ga neighbors, with the $O_h/T_d \sim 0.8/0.2$ ratio. This conclusion in Mn $2p$ XAS/XMCD of $Mn_{3-x}Co_xGa$ is consistent with those for the related Heulser alloys [22,24,27,28] and also qualitatively consistent with the Heusler structure of $Mn_{3-x}Co_xGa$ [see Fig. 1(b)]. Hence the Mn $2p$ XAS spectra of $Mn_{3-x}Co_xGa$ reveal that Mn ions are certainly divalent and that they have both the O_h and T_d local symmetries. Note that the finding of the divalency of Mn ions in $Mn_{3-x}Co_xGa$ refutes the Jahn-Teller effect being the origin of the structural transition in $Mn_{3-x}Co_xGa$ with increasing x [16].

Figure 3(c) compares the Mn $2p$ XMCD spectra of $Mn_{3-x}Co_xGa$ ($x = 0$, 0.17, 0.56, 0.77), the intensities of which are normalized to the Mn $2p_{3/2}$ XAS peaks. Note that, even though there are MnO impurities, the measured XMCD spectra of $Mn_{3-x}Co_xGa$ represent the instrisic features of $Mn_{3-x}Co_xGa$ because MnO would exhibits no XMCD signal due to the antiferromagnetic ground state of MnO. The Mn $2p$ XMCD intensities of $x = 0.17$ and 0 are very weak, indicating very weak spin polarization of Mn ions, in agreement with the very weak XMCD signals of Co $2p$ XMCD for $x = 0.17$ [see Fig. 2(f)]. Two major findings of Fig. 3(c) are as follows. (i) The line shapes of Mn $2p$ XMCD spectra are very similar to one another for different x values. (ii) The sign of Mn $2p$ XMCD signals is same as that of Co $2p$ XMCD. These findings indicate that both the valence and magnetic spin configurations of Mn ions do not change for varying x in $Mn_{3-x}Co_xGa$, and that the magnetic moments of Mn ions in $Mn_{3-x}Co_xGa$ are polarized due to the ordered magnetic moments of the substituted Co ions. The sign of the Mn $2p$ XMCD signals will be discussed under Fig. 3(d).
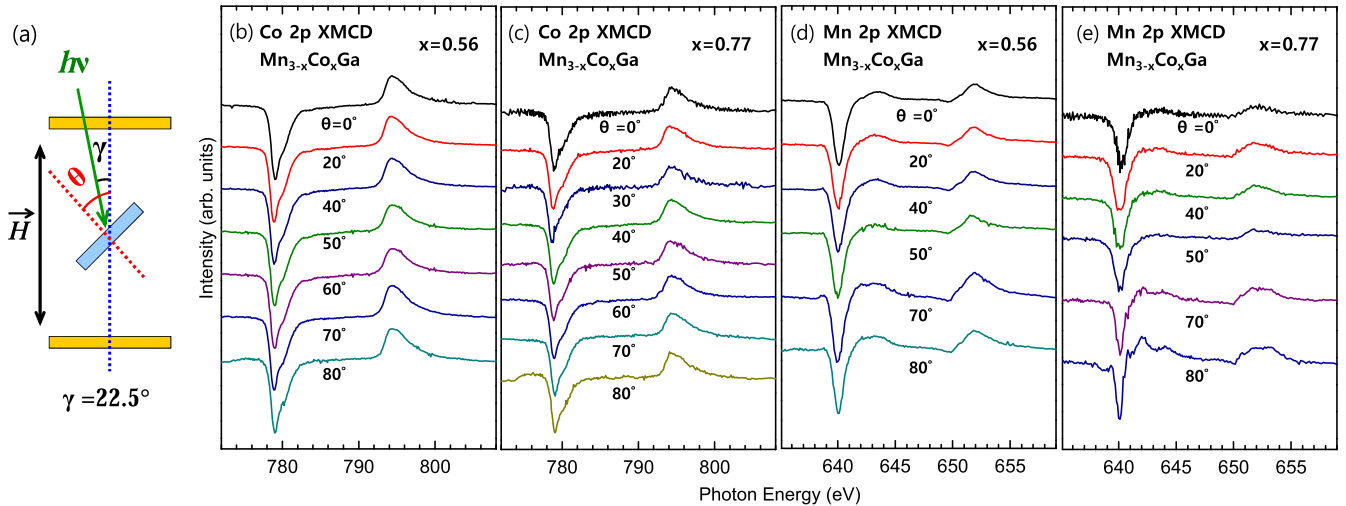
FIG. 4. Angle dependence of the XMCD spectra of $Mn_{3-x}Co_xGa$. (a) The experimental geometry of the angle-dependent XMCD measurement, where θ denotes the angle between the external magnetic field (**H**) and the sample surface normal, and γ denotes the angle between the incident photons and **H**. [(b) and (c)] Angle-dependent Co $2p$ XMCD spectra of $Mn_{3-x}Co_xGa$ with $x = 0.5$ and 0.77, respectively, for $0° \leqslant \theta \leqslant 80°$. [(d) and (e)] Similarly for Mn $2p$ XMCD spectra of $Mn_{3-x}Co_xGa$ with $x = 0.56$ and 0.77, respectively.

In order to determine the spin configurations of Mn ions in $Mn_{3-x}Co_xGa$, in Fig. 3(d), we have compared a representative Mn $2p$ XMCD spectrum of $Mn_{3-x}Co_xGa$ ($x = 0.56$) with those of reference Mn materials, such as nearly divalent (Mn^{2+}) $MnFe_2O_4$ ferrimagnetic spinel [40], trivalent (Mn^{3+}) $La_{1-3x}Ba_{3x}Mn_{1-x}Mo_xO_3$ perovskite ($x = 0.03$) [41], tetravalent (Mn^{4+}) La_2MnNiO_6 ferromagnetic double perovskite [42], and metallic Mn(1 monolayer)/Co(001) film [43]. The measured Mn $2p$ XMCD spectra of $Mn_{3-x}Co_xGa$ are found to be very similar to that of $Mn_{2.2}Co_{0.8}Ga$ [22]. Note that the multiplet features in Mn $2p$ XMCD of Co_2MnSi are sharper than those in $Mn_{2.2}Co_{0.8}Ga$ [22] and similar to those in $MnFe_2O_4$.

This comparison demonstrates that the Mn $2p$ XMCD spectrum of $Mn_{3-x}Co_xGa$ is quite different from those of other reference materials, except for divalent ferrimagnetic $MnFe_2O_4$, which confirms the divalent bonding states of Mn ions in $Mn_{3-x}Co_xGa$. On the other hand, the double-peak feature in the $2p_{1/2}$ (L_2) XMCD spectrum of $MnFe_2O_4$ is not observed in $Mn_{3-x}Co_xGa$. Further, the multiplet features in $Mn_{3-x}Co_xGa$ are broader than those in $MnFe_2O_4$, indicating the existence of weak covalent-bonding nature of Mn ions in $Mn_{3-x}Co_xGa$, compared to ionic bonding in $MnFe_2O_4$. Similarity in the XMCD of $Mn_{3-x}Co_xGa$ and Co_2MnSi [22] seems to support the divalent multiplet features in $Mn_{3-x}Co_xGa$.

The observed finite Mn $2p$ XMCD signals in $Mn_{3-x}Co_xGa$ for $x > 0$, despite the much weaker intensity of the Mn $2p$ XMCD than that of Co $2p$ XMCD (see Fig. 5), indicate that the magnetic moments of Mn ions are polarized due to ferromagnetic Co ions. In cubic Mn_3Ga, the magnetic moments of Mn ions in the different sublattices are considered to order oppositely to each other, resulting in a very small net magnetic moment [6]. Hence, the same sign of the Mn $2p$ XMCD signals as that of the Co $2p$ XMCD signals in $Mn_{3-x}Co_xGa$ [see Fig. 2(f)] suggests that the magnetic moments of Mn

ions are polarized along those of Co ions, resulting in the net magnetic moment along those of Co ions.

Previously it was shown that both the Mn $2p$ XAS and Mn $2p$ XMCD spectra of $MnFe_2O_4$ could be described by the

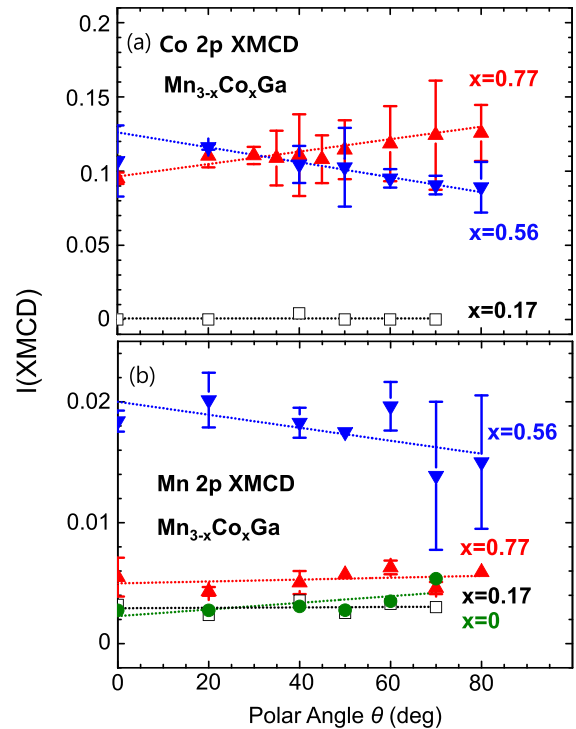

FIG. 5. Intensity plots of the measured XMCD spectra of $Mn_{3-x}Co_xGa$ for various polar angles between the external magnetic field and the sample surface normal. (a) The intensity plot of the Co $2p$ XMCD spectra of $Mn_{3-x}Co_xGa$ vs θ for $x = 0.77$, 0.56, 0.17. Similarly for (b) Mn $2p$ XMCD ($x = 0, 0.17, 0.56, 0.77$).
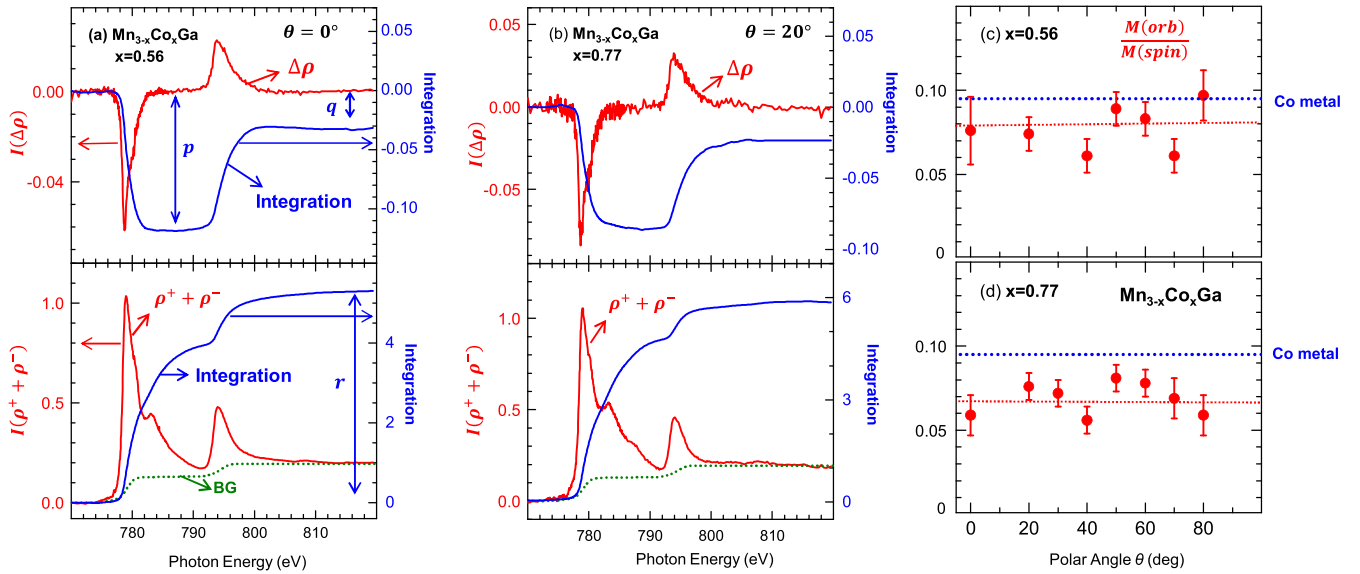
FIG. 6. Sum-rule analysis of the Co 2p XMCD spectra of $Mn_{3-x}Co_xGa$. (a) Co 2p XMCD spectrum (top) and XAS spectrum (bottom) of $Mn_{3-x}Co_xGa$ for $x = 0.56$ with $\theta = 0°$, with their integrations. Red curves of $\Delta\rho = \rho^+ - \rho^-$ (top) corresponds to the Co 2p XMCD, where ρ^+ and ρ^- denote the absorption spectra, obtained with different photon helicities. The blue curves represent the integration of $\Delta\rho$ (top), and the integration of $\rho^+ + \rho^-$ (bottom), after the background (green dotted curve) is removed. p, q and r are explained in the text under Eqs. (1) and (2). (b) Similarly for $x = 0.77$ with $\theta = 20°$. (c) The calculated ratio of $M(orb)/M(spin)$ vs the polar angle (θ) of $Mn_{3-x}Co_xGa$ for $x = 0.56$, where $M(orb)$ and $M(spin)$ denote the orbital magnetic moment and the spin magnetic moment, respectively. The red dotted line provides a guide line for the trend of $M(orb)/M(spin)$ vs θ. The blue dotted line represents $M(orb)/M(spin)$ of Co metal [20]. (d) Similarly for $x = 0.77$.

divalent Mn^{2+} states where T_d and O_h sites were mixed.[40] Hence, the similarity between the Mn 2p XMCD spectrum of $Mn_{3-x}Co_xGa$ and that of $MnFe_2O_4$ supports that the Mn ions in $Mn_{3-x}Co_xGa$ are nearly divalent and that the O_h-site Mn ions and the T_d-site Mn ions coexist in $Mn_{3-x}Co_xGa$, in agreement with the finding of Mn 2p XAS [see Fig. 3(b)]. On the other hand, the Mn 2p XMCD spectrum of $Mn_{3-x}Co_xGa$ is broader than that of $MnFe_2O_4$, which implies the existence of covalent-bonding character in $Mn_{3-x}Co_xGa$, different from $MnFe_2O_4$.

In the *bulk* magnetic property measurements for $Mn_{3-x}Co_xGa$ [16], a magnetic transition from hard ferrimagnetism with PMA to soft ferrimagnetism with IMA was observed with increasing Co content (x). In order to investigate the origin of the PMA-to-IMA magnetic transition in $Mn_{3-x}Co_xGa$, we have performed angle-dependent element-specific XMCD measurements for $Mn_{3-x}Co_xGa$. Figure 4 shows the angle dependence of the XMCD spectra of $Mn_{3-x}Co_xGa$ with respect to the external magnetic field. The experimental geometry of the angle-dependent XMCD measurement is drawn schematically in Fig. 4(a). Here θ denotes the polar angle between the applied magnetic field (**H**) and the sample surface normal. The angle γ denotes the angle between the incident photons and the applied magnetic field **H**, which is fixed to be $\gamma = 22.5°$ by the chamber geometry. In this geometry, the system with the PMA would exhibit stronger XMCD at $\theta \approx 0°$, while that with the IMA would exhibit stronger XMCD at $\theta \approx 90°$.

Figures 4(b) and 4(c) shown the angle-dependent Co 2p XMCD spectra of $Mn_{3-x}Co_xGa$ with $x = 0.56$ and 0.77, respectively, for $0° \leqslant \theta \leqslant 80°$. Similarly, Figs. 4(d) and 4(e)

show the angle-dependent Mn 2p XMCD spectra. In order to compare the line shapes, the XMCD spectra in Fig. 4 are scaled at the $2p_{3/2}$ peaks (negative peaks at $\sim$779 eV for Co 2p XMCD and $\sim$640 eV for Mn 2p XMCD). The intensities of I(XMCD), normalized to the corresponding $2p_{3/2}$ XAS peaks, are plotted in Fig. 5. Figure 4 reveals that the XMCD line shapes of both Co and Mn 2p states do not change with x and θ. The former implies that the electronic and spin configurations of both Co and Mn 3d states do not vary with x (the Co substitution), while the latter implies that the orbital to spin magnetic moments in $Mn_{3-x}Co_xGa$ do not change with polar angles (see Fig. 6 and Table I).

Figures 5(a) and 5(b) show the intensity plots of the Co and Mn 2p XMCD spectra of $Mn_{3-x}Co_xGa$ versus θ for $x = 0.77$, 0.56, 0.17, respectively. The intensities of the Co 2p XMCD are much stronger than those of the Mn 2p XMCD by an order of magnitude, implying that the contribution from the magnetic moments of Co ions is dominant over those of Mn ions. As θ increases, the Co 2p XMCD intensity increases slightly for $x = 0.77$, while it decreases slightly for $x = 0.56$. This trend indicates the IMA for $x = 0.77$ and the PMA for $x = 0.56$, which is consistent with the trend of the PMA-to-IMA transition with increasing Co content (x). In contrast, the Mn 2p XMCD intensities are rather independent of θ for all x, indicating that the magnetic properties of $Mn_{3-x}Co_xGa$ are determined mainly by the magnetic moments of Co ions but not much by the induced magnetic moments of Mn ions. These trends in Fig. 5, in combination with the findings of Fig. 2, reveal that the PMA-to-IMA magnetic transition in $Mn_{3-x}Co_xGa$ is determined mainly by the ferromagnetic metallic Co clusters of the substituted Co ions.

TABLE I. Co spin and orbital magnetic moments of $Mn_{3-x}Co_xGa$ for $x = 0.56$ ($\theta = 0°$) and $x = 0.77$ ($\theta = 20°$), obtained from the sum-rule analysis. Values of M(spin) and M(orb) are in units of μ_B/atom. Those values of Co metal were taken from Ref. [20].

$Mn_{3-x}Co_xGa$	M(spin)	M(orb)	M(orb)/M(spin)
$x = 0.56$	0.33	0.025	0.076
$x = 0.77$	0.42	0.032	0.076
Co metal (Ref. [20])	1.62	0.154	0.095

In order to quantify the orbital magnetic moments of Co ions in $Mn_{3-x}Co_xGa$ with polar angles, we have performed the sum-rule analysis of the Co $2p$ XMCD spectra of $Mn_{3-x}Co_xGa$ [44], the results of which are shown in Fig. 6. According to the XMCD sum rule, the element-specific spin magnetic moment M(spin) and orbital magnetic moment M(orb) can be determined from the measured XMCD spectra as follows:

$$M(\text{spin}) = -\frac{6p - 4q}{r}(10 - n_{3d})\left(1 + \frac{7\langle T_z \rangle}{2\langle S_z \rangle}\right)^{-1}, \quad (1)$$

$$M(\text{orb}) = -\frac{4q}{3r}(10 - n_{3d}), \quad (2)$$

where $p = \int_{L_3} \Delta\rho \, dE$, $q = \int_{L_3+L_2} \Delta\rho \, dE$, $r = \int_{L_3+L_2}(\rho^+ + \rho^-) \, dE$, $\Delta\rho = \rho^+ - \rho^-$. ρ^+, and ρ^- denote the absorption spectra, obtained with the right circular polarization and the left circular polarization, respectively. L_3 and L_2 in the lower bound of integrations denote the range of integration. n_{3d} is the $3d$ electron occupation number of the TM atom (Co atom here). In integrating $\rho^+ + \rho^-$, the background of $\rho^+ + \rho^-$ is removed. The definitions of p, q, and r are shown in Fig. 6(a). Here M(spin) and M(orb) are given in units of μ_B/atom. $\langle T_z \rangle$ is the expectation value of the magnetic dipole operator and $\langle S_z \rangle$ is equal to the half of M(spin) in Hartree atomic units. We have ignored the contribution of $\langle T_z \rangle$ [45]. For n_{3d}, the same value as for Co metal (i.e., $n_{3d} = 7.51$) [20] was used for $Mn_{3-x}Co_xGa$.

The top panel of Fig. 6(a) shows the Co $2p$ XMCD spectrum ($\Delta\rho$) of $Mn_{3-x}Co_xGa$ for $x = 0.56$ and $\theta = 0°$ (red) and its integration (blue). The bottom panel of Fig. 6(a) shows $\rho^+ + \rho^-$ (red) and its integration (blue), calculated after the background (green dotted curve) is removed. In Fig. 6(b) are shown similar results for $x = 0.77$ and $\theta = 20°$. The values obtained from the sum-rule analysis are shown in Table I. The magnitudes of M(spin) and M(orb) in $Mn_{3-x}Co_xGa$ are much smaller than those of Co metal[20], but the relative ratio of M(orb)/M(spin) in $Mn_{3-x}Co_xGa$ is of comparable magnitudes to that of Co metal. The magnitudes in $Mn_{3-x}Co_xGa$ (M(spin, Co ion) = 0.33–0.42 μ_B/atom for $x = 0.56$–0.77) are also smaller than those obtained by the SQUID magnetometry [M(spin) ~ 1 μ_B/atom for $x = 0.5$–0.8] [22] and those obtained by the VSM-SQUID magnetometry and calculations ($M_s \sim 1$–2 μ_B/unit cell for $x > 0.5$) [16]. The reason for the smaller magnitudes of M(spin) and M(orb) in $Mn_{3-x}Co_xGa$ in this work could be due to (i) the low external magnetic field (~ 0.7 T) and (ii) the room temperature measurement employed in this work.

In our $Mn_{3-x}Co_xGa$ XMCD, it was difficult to calculate r accurately because of the negative slopes of ρ^+ and ρ^- due to

the charging effect in $Mn_{3-x}Co_xGa$ in XMCD measurements. Nevertheless, such negative slopes cancel out each other in obtaining $\Delta\rho = \rho^+ - \rho^-$ (XMCD). Hence the relative ratio of M(orb)/M(spin) is reliable and meaningful even though the absolute values of M(spin) and M(orb), estimated from the sum rules, might not be precise. Therefore, for other polar angles in $Mn_{3-x}Co_xGa$, we have estimated M(orb)/M(spin) only using the following relation:

$$\frac{M(\text{orb})}{M(\text{spin})} = \frac{4q}{3(6p - 4q)}. \quad (3)$$

In Figs. 6(c) and 6(d), M(orb)/M(spin) versus θ for $x = 0.56$ and 0.77 respectively are plotted. The red dotted line provides a guide line for the trend of M(orb)/M(spin) versus θ. The blue dotted line represents M(orb)/M(spin) of Co metal [20]. These plots reveal that M(orb)/M(spin) in $Mn_{3-x}Co_xGa$ exhibits no particular trends with θ, supporting the findings of Figs. 4 and 5. Further, M(orb)/M(spin) in $Mn_{3-x}Co_xGa$ is slightly smaller than that of Co metal, indicating that the contribution of the orbital moments with respect to the spin moments in $Mn_{3-x}Co_xGa$ is smaller than in Co metal.

IV. CONCLUSION

In conclusion, by employing XAS and XMCD spectroscopies and the CT multiplet analysis of the measured XAS spectra, we have investigated the electronic structures and spin configurations of Co-substituted $Mn_{3-x}Co_xGa$ Heusler films. Co $2p$ XAS and XMCD spectra represent mainly ferromagnetic metallic Co clusters and a small amount of divalent Co ions with disordered magnetic moments in $Mn_{3-x}Co_xGa$, the latter of which correspond to the covalent-bonded Co ions substituted into the T_d sites for small x. Mn $2p$ XAS spectra show a partial oxidation of Mn ions in $Mn_{3-x}Co_xGa$ films, which occurs near the interface with the SiO_2 capping layer. Mn ions in $Mn_{3-x}Co_xGa$ are found to be nearly divalent with weak covalent-bonding nature, which reflects non-Jahn-Teller ions. Finite Mn $2p$ XMCD signals are observed for $x > 0$ in $Mn_{3-x}Co_xGa$, with the same sign as that of Co $2p$ XMCD, showing that the magnetic moments of Mn ions are polarized along the ordered magnetic moments of the substituted Co ions.

Angle-dependent Co $2p$ XMCD measurements show that, with increasing θ, the Co $2p$ XMCD intensity increases slightly for $x = 0.77$ but decreases slightly for $x = 0.56$, in agreement with the magnetic anisotropy transition from weak PMA to weak IMA with increasing x. The spin and orbital magnetic moments of Co ions in $Mn_{3-x}Co_xGa$ are estimated by using the sum-rule analysis, showing that M(orb)/M(spin)

ratios exhibit no particular trends with polar angles and with x and that the contribution of M(orb) is smaller than in Co metal. This work reveals that the PMA-to-IMA magnetic transition in $Mn_{3-x}Co_xGa$ is determined mainly by the ferromagnetic metallic Co clusters of the substituted Co ions.

[1] R. A. de Groot, F. M. Mueller, P. G. van Engen, and K. H. J. Buschow, Phys. Rev. Lett. **50**, 2024 (1983).

[2] S. Chadov, X. Qi, J. Kübler, G. H. Fecher, C. Felser, and S. C. Zhang, Nat. Mater. **9**, 541 (2010).

[3] H. Lin, L. A. Wray, Y. Xia, S. Xu, S. Jia, R. J. Cava, A. Bansil, and M. Z. Hasan, Nat. Mater. **9**, 546 (2010).

[4] T. Graf, C. Felser, and S. S. P. Parkin, Prog. Solid State Chem. **39**, 1 (2011).

[5] D. I. Bilc and P. Ghosez, Phys. Rev. B **83**, 205204 (2011).

[6] M. Hakimi, M. Venkatesan, K. Rode, K. Ackland, and J. M. D. Coey, J. Appl. Phys. **113**, 17B101 (2013).

[7] H. Kurt, K. Rode, H. Tokuc, P. Stamenov, M. Venkatesan, and J. M. D. Coey, Appl. Phys. Lett. **101**, 232402 (2012).

[8] A. K. Nayak, M. Nicklas, S. Chadov, P. Khuntia, C. Shekhar, A. Kalache, M. Baenitz, Y. Skourski, V. K. Guduru, A. Puri, U. Zeitler, J. M. D. Coey, and C. Felser, Nat. Mater. **14**, 679 (2015).

[9] R. Sahoo, L. Wollmann, S. Selle, T. Höche, B. Ernst, A. Kalache, C. Shekhar, N. Kumar, S. Chadov, C. Felser, S. S. P. Parkin, and A. K. Nayak, Adv. Mater. **28**, 8499 (2016).

[10] B. Balke, G. H. Fecher, J. Winterlik, and C. Felser, Appl. Phys. Lett. **90**, 152504 (2007).

[11] J. Winterlik, B. Balke, G. H. Fecher, C. Felser, M. C. M. Alves, and F. Bernardi, and J. Morais, Phys. Rev. B **77**, 054406 (2008).

[12] H. Kurt, K. Rode, M. Venkatesan, P. S. Stamenov, and J. M. D. Coey, Phys. Rev. B **83**, 020405(R) (2011).

[13] H. Kurt, K. Rode, M. Venkatesan, P. Stamenov, and J. M. D. Coey, Phys. Status Solidi B **248**, 2338 (2011).

[14] J. Winterlik, S. Chadov, A. Gupta, V. Alijani, T. Gasi, K. Filsinger, B. Balke, G. H. Fecher, C. A. Jenkins, F. Casper, J. Kübler, G.-D. Liu, L. Gao, S. S. P. Parkin, and C. Felser, Adv. Mater. **24**, 6283 (2012).

[15] S. Chadov, S. W. D'Souza, L. Wollmann, J. Kiss, G. H. Fecher, and C. Felser, Phys. Rev. B **91**, 094203 (2015).

[16] K. Lee, W. Yoo, Q. A. T. Nguyen, H.-W. Bang, H. Kim, M. Kläui, S. H. Rhim, and M.-H. Jung, J. Alloys Compd. **858**, 158288 (2021).

[17] F. M. F. de Groot, J. C. Fuggle, B. T. Thole, and G. A. Sawatzky, Phys. Rev. B **42**, 5459 (1990).

[18] G. van der Laan and I. W. Kirkman, J. Phys.: Condens. Matter **4**, 4189 (1992).

[19] B. T. Thole, P. Carra, F. Sette, and G. van der Laan, Phys. Rev. Lett. **68**, 1943 (1992).

[20] C. T. Chen, Y. U. Idzerda, H.-J. Lin, N. V. Smith, G. Meigs, E. Chaban, G. H. Ho, E. Pellegrin, and F. Sette, Phys. Rev. Lett. **75**, 152 (1995).

[21] J.-H. Park, E. Vescovo, H.-J. Kim, C. Kwon, R. Ramesh, and T. Venkatesan, Phys. Rev. Lett. **81**, 1953 (1998).

[22] P. Klaer, C. A. Jenkins, V. Alijani, J. Winterlik, B. Balke, C. Felser, and H. J. Elmers, Appl. Phys. Lett. **98**, 212510 (2011).

[23] Y. Seo, S. Seong, and J.-S. Kang, J. Kor. Mag. Soc. **32**, 1 (2022).

[24] S. Ouardi, G. H. Fecher, T. Kubota, S. Mizukami, E. Ikenaga, T. Nakamura, and C. Felser, J. Phys. D: Appl. Phys. **48**, 164007 (2015).

[25] K. Rode, N. Baadji, D. Betto, Y.-C. Lau, H. Kurt, M. Venkatesan, P. Stamenov, S. Sanvito, J. M. D. Coey, E. Fonda, E. Otero, F. Choueikani, P. Ohresser, F. Porcher, and G. Andre, Phys. Rev. B **87**, 184429 (2013).

[26] S. Seong, E. Lee, H. Y. Kim, Y. Kim, J. Baik, and J.-S. Kang, Curr. Appl. Phys. **18**, 1190 (2018).

[27] Y. B. Xu, S. S. A. Hassan, P. K. J. Wong, J. Wu, J. S. Claydon, Y. X. Lu, C. D. Damsgaard, J. B. Hansen, C. S. Jacobsen, Y. Zhai, G. van der Laan, R. Feidenhans, and S. N. Holmes, IEEE Trans. Magn. **44**, 2959 (2008).

[28] J. Winterlik, G. H. Fecher, B. Balke, T. Graf, V. Alijani, V. Ksenofontov, C. A. Jenkins, O. Meshcheriakova, C. Felser, G. Liu, S. Ueda, K. Kobayashi, T. Nakamura, and M. Wojcik, Phys. Rev. B **83**, 174448 (2011).

[29] There was a charging problem in XAS/XMCD measurements of $Mn_{3-x}Co_xGa$ films. So it was difficult to obtain good XAS and XMCD spectra at low temperature ($T \sim 80$ K). Hence we present the room-temperature (RT) XAS and XMCD data in this paper.

[30] T. J. Regan, H. Ohldag, C. Stamm, F. Nolting, J. Lüning, J. Stöhr, and R. L. White, Phys. Rev. B **64**, 214422 (2001).

[31] A. Singh, H. Y. Huang, Y. Y. Chin, Y. F. Liao, T. C. Huang, J. Okamoto, W. B. Wu, H. J. Lin, K. D. Tsuei, R. P. Wang, F. M. F. de Groot, C. N. Kuo, H. F. Liu, C. S. Lue, C. T. Chen, D. J. Huang, and A. Chainani, Phys. Rev. B **98**, 235136 (2018).

[32] J.-S. Kang, S. S. Lee, G. Kim, H. J. Lee, H. K. Song, Y. J. Shin, S. W. Han, C. Hwang, M. C. Jung, H. J. Shin, B. H. Kim, S. K. Kwon, and B. I. Min, Phys. Rev. B **76**, 195122 (2007).

[33] The software for the cluster model calculations used in the work is the CTM4XAS program, which was provided by F. M. F. de Groot.

[34] F. M. F. de Groot, Coord. Chem. Rev. **249**, 31 (2005).

[35] H. Ikeno, F. M. F. de Groot, E. Stavitski, and I. Tanaka, J. Phys.: Condens. Matter **21**, 104208 (2009).

[36] J. Lee, B. Kim, B. H. Kim, B. I. Min, S. Kolesnik, O. Chmaissem, J. Mais, B. Dabrowski, H. J. Shin, D. H. Kim, H. J. Lee, and J.-S. Kang, Phys. Rev. B **80**, 205112 (2009).

[37] C. Mitra, Z. Hu, P. Raychaudhuri, S. Wirth, S. I. Csiszar, H. H. Hsieh, H.-J. Lin, C. T. Chen, and L. H. Tjeng, Phys. Rev. B **67**, 092404 (2003).

[38] J.-S. Kang, G. Kim, S. C. Wi, S. S. Lee, S. Choi, Sunglae Cho, S. W. Han, K. H. Kim, H. J. Song, H. J. Shin, A. Sekiyama,

S. Kasai, S. Suga, and B. I. Min, Phys. Rev. Lett. **94**, 147202 (2005).

[39] P. Ghigna, A. Campana, A. Lascialfari, A. Caneschi, D. Gatteschi, A. Tagliaferri, and F. Borgatti, Phys. Rev. B **64**, 132413 (2001).

[40] J.-S. Kang, G. Kim, H. J. Lee, D. H. Kim, H. S. Kim, J. H. Shim, S. Lee, H. G. Lee, J.-Y. Kim, B. H. Kim, and B. I. Min, Phys. Rev. B **77**, 035121 (2008).

[41] Our data (unpublished).

[42] J.-S. Kang, H. J. Lee, D. H. Kim, S. Kolesnik, B. Dabrowski, K. Świerczek, Jieun Lee, Bongjae Kim, and B. I. Min, Phys. Rev. B **80**, 045115 (2009).

[43] W. L. O'Brien and B. P. Tonner, Phys. Rev. B **50**, 2963 (1994).

[44] We have not performed the sum-rule analysis for Mn $2p$ XMCD data because the absolute intensites of Mn $2p$ XMCD are much smaller than those of Co $2p$ XMCD ($\sim$1/10 of Co $2p$ XMCD). See Fig. 5.

[45] T. Oguchi and T. Shishidou, Phys. Rev. B **70**, 024412 (2004).